

pubs.acs.org/JPCB Article

Characterizing the Interplay between Polymer Solvation and Conformation

Published as part of The Journal of Physical Chemistry virtual special issue "Lawrence R. Pratt Festschrift". Debdas Dhabal, Zhitong Jiang, Akash Pallath, and Amish J. Patel*



Cite This: J. Phys. Chem. B 2021, 125, 5434-5442



ACCESS

Metrics & More



Polymer size

Supporting Information

Solvation co-ordinate

Dry

ABSTRACT: Conformational transitions of flexible molecules, especially those driven by hydrophobic effects, tend to be hindered by desolvation barriers. For such transitions, it is thus important to characterize and understand the interplay between solvation and conformation. Using specialized molecular simulations, here we perform such a characterization for a hydrophobic polymer solvated in water. We find that an external potential, which unfavorably perturbs the polymer hydration waters, can trigger a coil-toglobule or collapse transition, and that the relative stabilities of the collapsed and extended states can be quantified by the strength of the requisite potential. Our results also provide mechanistic insights into the collapse transition, highlighting that the bottleneck to polymer collapse is the formation of a sufficiently large cluster, and the collective dewetting of such a cluster. We also study the collapse of the hydrophobic polymer in octane, a nonpolar solvent, and interestingly, we find that the mechanistic details of the transition are qualitatively similar to that in water.

1. INTRODUCTION

Aqueous or organic solutions of conformationally flexible solutes, such as polymers or peptides, play an important role in diverse materials^{1–5} and biomolecular contexts.^{6–9} Although solvated flexible molecules can exist in a multitude of conformations, they often display two or more distinct basins that are separated by free energy barriers, e.g., polymers can be in extended or collapsed states, whereas proteins can be in their native folded structures, become denatured, or even adopt well-defined misfolded configurations.^{10–12} Molecular simulations have been extensively used, often with the aid of enhanced sampling methods, to characterize the conformational free energy landscapes of diverse flexible molecules, typically as a function of solute coordinates, such as radius of gyration or dihedral angles.^{8,13}

In characterizing such landscapes, solvent degrees of freedom are usually integrated out. When solvent degrees of freedom equilibrate rapidly with respect to the solute coordinates, such integration does not lead to any loss of mechanistic information into conformational transitions. However, certain transitions, such as those driven by hydrophobic effects, tend to feature slow solvent degrees of freedom, which relax on time scales that are comparable to, or even longer than, the relaxation times of the solute coordinates. In particular, both theoretical and simulation studies have highlighted the importance of slow solvent degrees of freedom in the coil-to-globule transition of nonpolar polymers in water.

For transitions featuring slow solvent degrees of freedom, attempts to integrate out the solvent coordinates can lead to hysteresis in the sampling of the solute coordinates and make it challenging to accurately estimate the conformational free energy landscape.²⁴ Importantly, the resulting loss of mechanistic information can also obfuscate how the conformational landscape might respond to changes in the solvent, e.g., due to the introduction of cosolutes 25-28 or proximity to interfaces.^{29–33} Thus, characterizing the interplay between conformation and solvation, e.g., through a free energy landscape that is a function of both solute and solvent coordinates, can be valuable, particularly for systems that are expected to feature slow solvent degrees of freedom. 15,16,34 However, the enhanced sampling of solvent coordinates, which must be performed to obtain such a landscape, can be challenging because the solvation shell of a flexible solute is inherently dynamic and changes along with the conformation of the solute.

To address this challenge, we recently introduced a method for sampling the number of solvent molecules, \tilde{N}_{ν} , in a dynamical volume, ν , which evolves with, and continuously

 Received:
 March 10, 2021

 Revised:
 May 4, 2021

 Published:
 May 12, 2021





conforms to, the shape of a flexible solute of interest.³⁴ Here, we use this method to study the coil-to-globule or collapse transition of a flexible hydrophobic polymer solvated in water. We find that polymer collapse can be triggered by an unfavorable potential, $\phi ilde{N}_{v}$, that perturbs the polymer hydration waters, 35,36 and that the potential strength, ϕ , needed to trigger the transition can serve as a measure of the relative stabilities of the collapsed and extended states. We also characterize the free energy landscape as a function of both the radius of gyration of the polymer (solute coordinate), and the number of waters, \tilde{N}_{ν} , in its hydration shell (solvent coordinate), and use this characterization to uncover mechanistic insights into the collapse transition. We find that the bottleneck to polymer collapse is the formation of a sufficiently large nonpolar cluster, which must undergo dewetting for the collapse transition to proceed. 15,16 We also study the collapse of the hydrophobic polymer in the nonpolar solvent, octane, and find that it is remarkably similar to the collapse of the polymer in water.

2. METHODS

To interrogate the interplay between the solvation and conformation of flexible solutes, here we study a linear alkane chain consisting of 45 beads that is designated as C₄₅. The solvation shell, v, of the C₄₅ chain, is defined as the union of 45 spherical subvolumes with radius, r_{ν} , which are pegged to the C_{45} monomers. Thus, the solvation shell, ν , of the flexible C_{45} molecule is not static but changes its shape and/or size dynamically in response to the conformational fluctuations of the polymer. Using the recently developed dynamic INDUS method,³⁴ here we bias the coarse-grained number, \tilde{N}_{ν} , of solvent heavy atoms in ν ; \tilde{N}_{ν} is closely related to the actual number of solvent atoms in ν but is chosen to be a continuous function of particle positions to permit biasing \tilde{N}_{ν} without resulting in impulsive forces. 37,38 By using harmonic biasing potentials to sample \tilde{N}_{ν} over its range of interest and using the weighted histogram analysis method (WHAM) to combine the biased probability distributions, 39-42 we are able to characterize the free energetics, $\beta G_{\nu}(\tilde{N}) \equiv -\ln P_{\nu}(\tilde{N})$, where $\beta^{-1} \equiv k_{\rm B}T$ is the thermal energy, and $P_{\nu}(\tilde{N})$ is the probability of observing \tilde{N} solvent atoms in ν . The probability, $P_{\nu}(\tilde{N}) \equiv \langle \delta(\tilde{N} - \tilde{N}_{\nu}) \rangle_{0}$, is the ensemble average of the Dirac delta function obtained using the unbiased Hamiltonian, \mathcal{H}_0 . Once $G_{\nu}(\tilde{N})$ is estimated, we use standard reweighting techniques³⁹ to interrogate how biasing potentials, such as $U_{\phi} \equiv \phi \tilde{N}_{\nu}$, modulate polymer solvation and determine the corresponding averages, $\langle \cdots \rangle_{dn}$ obtained using the biased Hamiltonians, $\mathcal{H}_{\phi} = \mathcal{H}_0 + U_{\phi}$. For example, the free energetics in a biased ensemble, $\beta G_{\nu}^{\phi}(\tilde{N}) \equiv -\ln P_{\nu}^{\phi}(\tilde{N})$, can be obtained using $P_{\nu}^{\phi}(\tilde{N}) \equiv$ $\langle \delta(\tilde{N} - \tilde{N}_{\nu}) \rangle_{\phi}$. Finally, to characterize the two-dimensional free energetics, $\beta G_{\nu}(\tilde{N}, R_{g}) \equiv -\ln P_{\nu}(\tilde{N}, R_{g})$, where $P_{\nu}(\tilde{N}, R_{\sigma})$ is the joint probability of observing \tilde{N} solvent atoms in ν , and the polymer with a radius of gyration, R_g , we combine the joint probability distributions, observed in our biased simulations, using the WHAM weights determined above. 38,43

2.1. Simulation Details. All simulations were performed using the GROMACS package⁴⁴ (version 4.5.3), suitably modified to perform indirect umbrella sampling (INDUS)

using dynamic probe volumes. 34,38 The equations of motion were integrated using the leapfrog algorithm with a time step of 2 fs, and periodic boundary conditions were employed in all three dimensions. The system temperature, T, was maintained at 298 K using the canonical velocity rescaling thermostat⁴⁵ with a time constant of 0.5 ps, and the system pressure, P, was maintained at 1 atm using the Parrinello-Rahman barostat⁴⁶ with a time constant of 1 ps. The *n*-alkane chain containing 45 carbons (designated as C₄₅) was modeled using the TraPPE-UA (transferable potentials for phase equilibria-united atom) force field developed by Siepmann et al. 47 The TraPPE-UA force field models individual -CH2- or -CH3 units as pseudoatoms, so that our solute is composed of 45 unitedatom beads. The C₄₅ chain was solvated using either water or n-octane, and Lorentz-Berthelot combination rules were used to determine the Lennard-Jones parameters for crossinteractions. In all cases, the simulation box was first energy minimized using the steepest descent algorithm, followed by a 2 ns NVT simulation, and then a 4 ns NPT simulation to equilibrate the system. The biased simulations were run for 10 ns, with either the first 2 ns (for C_{45} /water) or 1 ns (for C_{45} / octane) being discarded for equilibration; the coarse-grained number of solvent atoms, \tilde{N}_{v} , in the polymer solvation shell, v_{v} and the polymer radius of gyration, Rg, were estimated every 0.1 ps. Additional details of the C_{45} /water and C_{45} /octane simulations are included below.

 $C_{45}/Water$. Water was modeled using the SPC/E (extended simple point charge) model⁴⁸ with bonds involving hydrogen atoms being constrained using the SETTLE algorithm.⁴⁹ The particle mesh Ewald (PME) method⁵⁰ was used to compute long-range electrostatic interactions; short-range electrostatic and Lennard-Jones interactions were truncated at 1 nm. The C_{45} chain was hydrated using 11 614 water molecules giving rise to a roughly 7 nm cubic simulation box. Before biased simulations were performed, a 10 ns long unbiased simulation was performed to estimate the average number of solvent atoms in ν and ascertain the \tilde{N}_{ν} range that must be sampled; the radius of the spherical subvolumes used to define ν was chosen to be $r_{\nu}=0.6$ nm. The biased simulations used harmonic potentials with a spring constant of 0.0243 kJ/mol.

 $C_{45}/Octane$. Octane was modeled using the TraPPE-UA force field⁴⁷ with Lennard-Jones interactions being truncated at 1.4 nm. The C_{45} chain was solvated using 1000 octane molecules. The subvolume radius used to define ν was chosen to be $r_{\nu}=0.7$ nm, and a spring constant of 0.033 kJ/mol was used for the harmonic biasing potentials.

Characterizing Localized Solvation. To determine the solvation state of a bead (with index i) in a particular configuration, we estimate the (discrete) number of solvent heavy atoms, n_i , in the spherical subvolume of radius, r_v , centered on the bead. We then compare n_i against a fixed threshold, \overline{n}_i , to determine whether bead i is well-solvated; the bead is considered to be solvated for $n_i \geq \overline{n}_i$, whereas it is deemed to be desolvated for $n_i < \overline{n}_i$. The threshold, \overline{n}_i , is defined as $\overline{n}_i \equiv (\overline{n}_i^C + \overline{n}_i^E)/2$, where \overline{n}_i^C and \overline{n}_i^E are the average values of n_i in the collapsed and extended basins, respectively. To estimate \overline{n}_i^C and \overline{n}_i^E , we use our biased simulations that best sample the collapsed and extended basins, respectively.

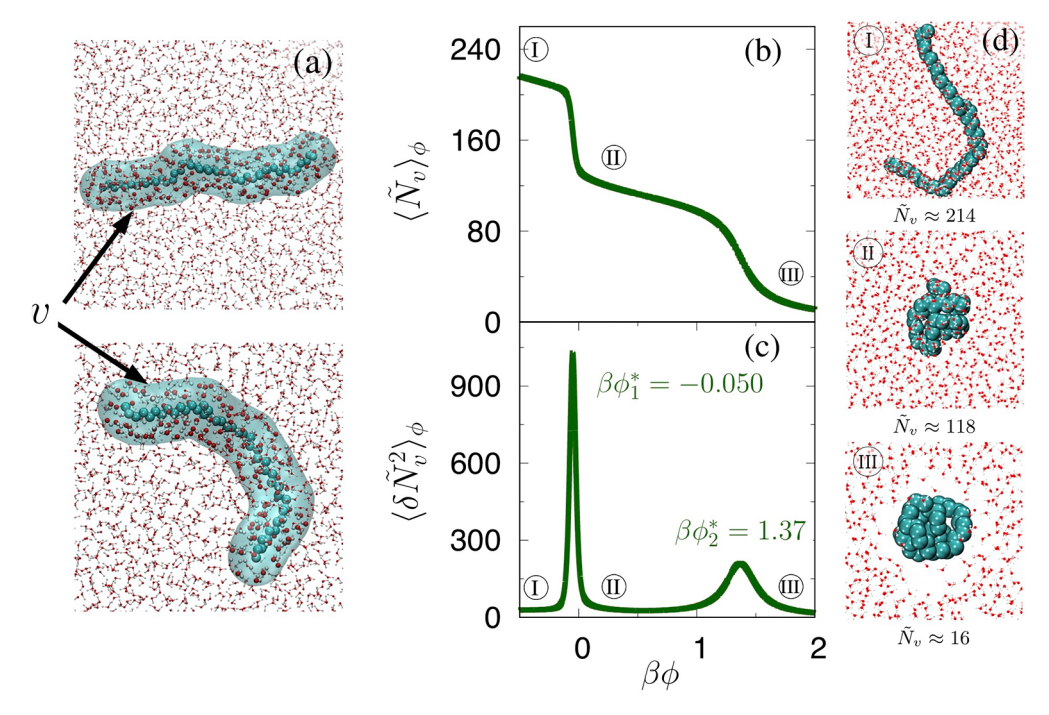


Figure 1. (a) Simulation snapshots of the C_{45} polymer (cyan, space-fill) solvated in water (red/white) are shown. Water molecules in the polymer hydration shell, ν (cyan, transparent), are highlighted. As the conformation of the polymer fluctuates, so does the shape and size of its hydration shell; to account for such fluctuations, ν is defined to be the union of 45 spherical subvolumes that are centered on the polymer beads and have radii, $r_{\nu} = 0.6$ nm. (b) As the strength, ϕ , of a linear biasing potential, $U_{\phi} = \phi \tilde{N}_{\nu}$, is increased, the average number of waters, $\langle \tilde{N}_{\nu} \rangle_{\phi}$, in the hydration shell decreases; interestingly, two sharp drops are observed in $\langle \tilde{N}_{\nu} \rangle_{\phi}$. (c) Correspondingly, the susceptibility, $-\partial \langle \tilde{N}_{\nu} \rangle_{\phi} / \partial (\beta \phi) = \langle \delta \tilde{N}_{\nu}^2 \rangle_{\phi}$, displays two peaks at ϕ -values denoted by ϕ_1^* and ϕ_2^* . (d) Simulation snapshots corresponding to three select \tilde{N}_{ν} -values are shown. As shown in snapshot I, the polymer adopts an extended configuration for $\tilde{N}_{\nu} > \langle \tilde{N}_{\nu} \rangle_{\phi_1^*}$, whereas snapshot II highlights that the polymer is in a collapsed configuration for $\langle \tilde{N}_{\nu} \rangle_{\phi_2^*} < \tilde{N}_{\nu} < \langle \tilde{N}_{\nu} \rangle_{\phi_2^*}$. As illustrated in snapshot III, the collapsed polymer is dewetted for $\tilde{N}_{\nu} < \langle \tilde{N}_{\nu} \rangle_{\phi_2^*}$.

3. RESULTS AND DISCUSSION

3.1. How Polymer Hydration Waters Respond to Perturbations. To characterize how the hydration of the flexible C₄₅ chain influences its conformation, we focus on water molecules in its first hydration shell, ν (Figure 1a, cyan/ transparent). We account for the dynamic nature of the polymer hydration shell, i.e., changes in its size and shape, by defining ν to be the union of 45 spherical subvolumes, where every subvolume is pegged to a polymer bead and has a radius, $r_v = 0.6$ nm. We then interrogate how the polymer hydration waters respond to perturbations by employing a biasing potential, $U_{\phi} = \phi \tilde{N}_{\nu}$, where \tilde{N}_{ν} is the (coarse-grained) number of waters in ν , and ϕ is the potential strength. Such a biasing potential provides a convenient way to modulate \tilde{N}_{ν} , and thereby polymer hydration. In particular, hydration is disfavored for $\phi > 0$ with the perturbation becoming more pronounced as ϕ is increased; conversely, polymer hydration is favored for ϕ < 0. From a physical standpoint, a potential of strength, ϕ , decreases the effective pressure in the polymer hydration shell by roughly $\phi \rho_{\rm w}$, where $\rho_{\rm w}$ is the density of bulk water.51

The response of the C_{45} hydration waters to the biasing potential is shown in Figure 1. As expected, the average number of hydration waters, $\langle \tilde{N}_{\nu} \rangle_{\phi}$, decreases as ϕ is increased (Figure 1b). However, the decrease in $\langle \tilde{N}_{\nu} \rangle_{\phi}$ is not gradual but is punctuated by two sharp drops. The corresponding susceptibility, $\partial \langle \tilde{N}_{\nu} \rangle_{\phi} / \partial (-\beta \phi) = \langle \delta \tilde{N}_{\nu}^2 \rangle_{\phi}$, shown in Figure

1c, displays marked peaks at ϕ -values, which are denoted by ϕ_1^* and ϕ_2^* . The sharp drops in $\langle \tilde{N}_{\nu} \rangle_{\phi}$, and the corresponding peaks in susceptibility, suggest that the polymer undergoes collective transitions at potential strengths, ϕ_1^* and ϕ_2^* . To shed light on the nature of these transitions, we include representative snapshots of the system for select \tilde{N}_{ν} -values in Figure 1d. Snapshot I suggests that the polymer is in an extended configuration for $\phi < \phi_1^*$; snapshot II shows the polymer in a collapsed but hydrated configuration for $\phi_1^* < \phi < \phi_2^*$, and snapshot III highlights that the collapsed polymer is dewetted for $\phi > \phi_2^*$. These snapshots suggest that, at potential strength ϕ_1^* , the polymer undergoes a collapse (or folding) transition, whereas, at potential strength ϕ_2^* , the collapsed polymer dewets.

3.2. Interplay between Polymer Hydration and Conformation. To characterize the free energy landscape underpinning the collapse and dewetting transitions, we estimate the free energetics, $G_{\nu}(\tilde{N})$, of water number fluctuations in the hydration shell of the C_{45} polymer (Figure 2a), as well as the corresponding two-dimensional free energy landscape, $G_{\nu}(\tilde{N}, R_{\rm g})$ (Figure 2b). The conformational free energy landscape, $G_{\nu}(R_{\rm g})$, can be readily obtained from $G_{\nu}(\tilde{N}, R_{\rm g})$ by integrating out \tilde{N} and is included in Figure S1 of the Supporting Information. Figure 2 confirms the presence of two nearly degenerate basins, observed at low $\tilde{N} \approx 130$ and

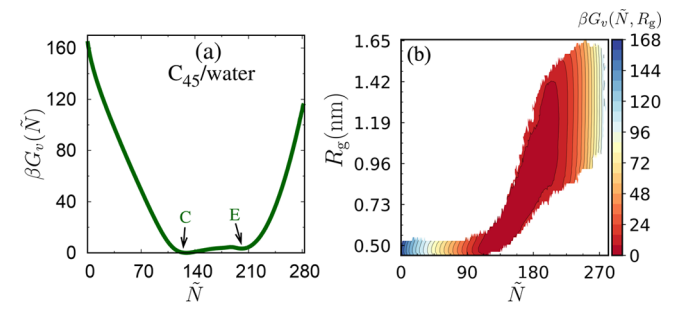


Figure 2. (a) Free energetics of water number fluctuations, $G_{\nu}(\tilde{N})$, in the dynamical hydration shell of the C_{45} polymer are shown. The basins corresponding to the collapsed (C) and extended (E) states of the polymer are denoted with arrows. (b) To illustrate the interplay between the hydration of the hydrophobic polymer in water and its conformation, we plot the two-dimensional free energy landscape, $G_{\nu}(\tilde{N}, R_{\rm g})$, where \tilde{N} is the number of waters in ν , and $R_{\rm g}$ is the radius of gyration of the C_{45} polymer. The relatively sharp increase in $G_{\nu}(\tilde{N}, R_{\rm g})$ at low \tilde{N} and $R_{\rm g}$ corresponds to the free energetic cost of dewetting the collapsed polymer globule, whereas the increase in $G_{\nu}(\tilde{N}, R_{\rm g})$ at high \tilde{N} and $R_{\rm g}$ corresponds to the unfavorable wetting of the extended polymer.

 $R_{\rm g}\approx 0.5$ nm, and at higher $\tilde{N}\approx 200$ and $R_{\rm g}\approx 1.2$ nm, corresponding to the collapsed (C) and extended (E) states, respectively. Figure 2 also suggests that the solvation and conformational coordinates are coupled to one another across the collapse transition, and that the transition incurs a free energetic cost of less than $8k_{\rm B}T$. In contrast, decreasing \tilde{N} below 100 results in a sharp increase in $G_{\nu}(\tilde{N},R_{\rm g})$; such a decrease in \tilde{N} is not accompanied by a further decrease in $R_{\rm g}$, suggesting that it corresponds to the dewetting of the collapsed polymer. Similarly, increasing \tilde{N} above 220 also incurs a large free energetic penalty and is not accompanied by an increase in $R_{\rm g}$, suggesting that it represents the unfavorable compression of waters in the hydration shell of the extended polymer.

Although the free energy difference between the collapsed and extended states, i.e., the folding free energy, ΔG_{fold} , is relatively small, Figure 2a suggests that, for the hydrophobic C₄₅ chain in water, the collapsed state is nevertheless stable relative to the extended state, with $\beta \Delta G_{\text{fold}} = -3.3$. The relative stability of the collapsed state is also evident from the fact that the potential strength, ϕ_1^* , corresponding to the collapse transition is negative (Figure 1c). In fact, the two quantities are proportional to one another, with $\Delta G_{\text{fold}} \approx \phi_1^* (\tilde{N}_{\text{E}} - \tilde{N}_{\text{C}})$, where $\tilde{N}_{\rm E}$ and $\tilde{N}_{\rm C}$ are \tilde{N} -values corresponding to the extended and collapsed basins, respectively. Because the collapsed and extended states are expected to be in coexistence with one another in the ϕ_1^* -ensemble, i.e., $G_{\nu}^{\phi_1^*}(\tilde{N}_{\rm C}) = G_{\nu}^{\phi_1^*}(\tilde{N}_{\rm E})$, and because $G_v^{\phi}(\tilde{N})$ equals $G_v(\tilde{N}) + \phi \tilde{N}$ within a constant, 43 we obtain $G_{\nu}(\tilde{N}_{\rm C}) + \phi_1^* \tilde{N}_{\rm C} = G_{\nu}(\tilde{N}_{\rm E}) + \phi_1^* \tilde{N}_{\rm E}$. Thus, the polymer folding free energy, $\Delta G_{\text{fold}} \approx G_{\nu}(\tilde{N}_{\text{C}}) - G_{\nu}(\tilde{N}_{\text{E}}) =$ $\phi_1^*(\tilde{N}_E - \tilde{N}_C)$. For the C₄₅ polymer in water, we estimate $\phi_1^*(\tilde{N}_{\rm E}-\tilde{N}_{\rm C})\approx -3.47k_{\rm B}T$, which in good agreement with ΔG_{fold} obtained directly from $G_{\nu}(\tilde{N})$. Thus, ϕ_1^* can serve as a quantitative measure of ΔG_{fold} .

3.3. Free Energy Landscape at the Collapse Transition. To better understand the transition of the C_{45} polymer

between its extended and collapsed states, we now focus on its behavior in the presence of a biasing potential of strength, ϕ_1^* , wherein the two states are expected to be in coexistence with one another. The corresponding free energy landscapes, $G_{\nu}^{\phi_1^*}(\tilde{N})$ and $G_{\nu}^{\phi_1^*}(\tilde{N}, R_{\rm g})$, are shown in Figure 3. As seen in

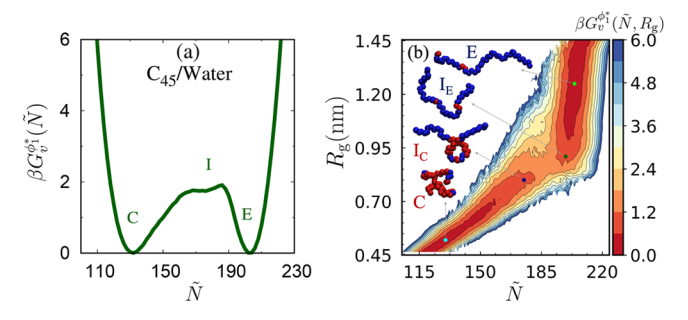


Figure 3. To better understand the coil-to-globule collapse transition of the C_{45} polymer, here we study its behavior in the ϕ_1^* -ensemble, that is, in the presence of the biasing potential, $\phi_1^* \tilde{N}_{\nu}$, where $\beta \phi_1^* = -0.05$. In such a biased ensemble, the coil and globule states are expected to be in coexistence with one another. (a) The free energetics, $G_{\nu}^{\phi_1^*}(\tilde{N})$, of water number fluctuations in the ϕ_1^* -ensemble, display two distinct basins that are separated by a barrier of roughly $2k_{\rm B}T$. The basins corresponding to the collapsed (low \tilde{N}) and extended (high \tilde{N}) states of the polymer are labeled C and E, respectively, whereas the location of the maximum in $G_{\nu}^{\phi_1^*}(\tilde{N})$ at intermediate \tilde{N} is denoted by I. (b) The two-dimensional free energy landscape in the ϕ_1^* -ensemble, $G_{\nu}^{\phi_1^*}(\tilde{N}, R_g)$, sheds light on the minimum free energy path that the polymer is likely to adopt as it undergoes collapse. Representative configurations of the polymer in the collapsed basin (C), transition regions, I_E and I_C, and the extended basin (E) are also shown. In these snapshots, hydrated polymer beads are colored blue, whereas those that are dehydrated are colored red.

Figure 3a, $G_{\nu}^{\phi_1^*}(\tilde{N})$ features two basins: the low- \tilde{N} , collapsed (C), and the high- \tilde{N} , extended (E), basins, which are in coexistence with one another and are separated by an intermediate- \tilde{N} (I) barrier of roughly $2k_{\rm B}T$. In Figure 3b, we plot the two-dimensional free energy landscape, $G_{\nu}^{\phi_1^*}(\tilde{N}, R_{\sigma})$, which sheds light on the pathways that the polymer might follow as it undergoes the collapse transition; i.e., it elucidates the minimum free energy path in the (\tilde{N}, R_{σ}) space, with \tilde{N} and R_g representing the polymer hydration and conformational degrees of freedom. The $G_{\nu}^{\phi_1^*}(\tilde{N},R_{\rm g})$ landscape highlights that, in its extended state, the polymer can undergo substantial fluctuations in R_g but only small fluctuations in \tilde{N} . The polymer can thus approach the saddle point in $G_{\nu}^{\phi_1^*}(\tilde{N},R_{g})$ through a marked low- R_{σ} fluctuation wherein it retains most of its hydration waters. However, to traverse the saddle point region, the polymer must undergo a substantive decrease in \tilde{N} , losing a number of its hydration waters with only a small decrease in R_g . Upon crossing the saddle point region, the polymer then collapses through a coordinated decrease in both

Figure 3b also includes representative simulation snapshots of the polymer in the extended basin (E), the transition region

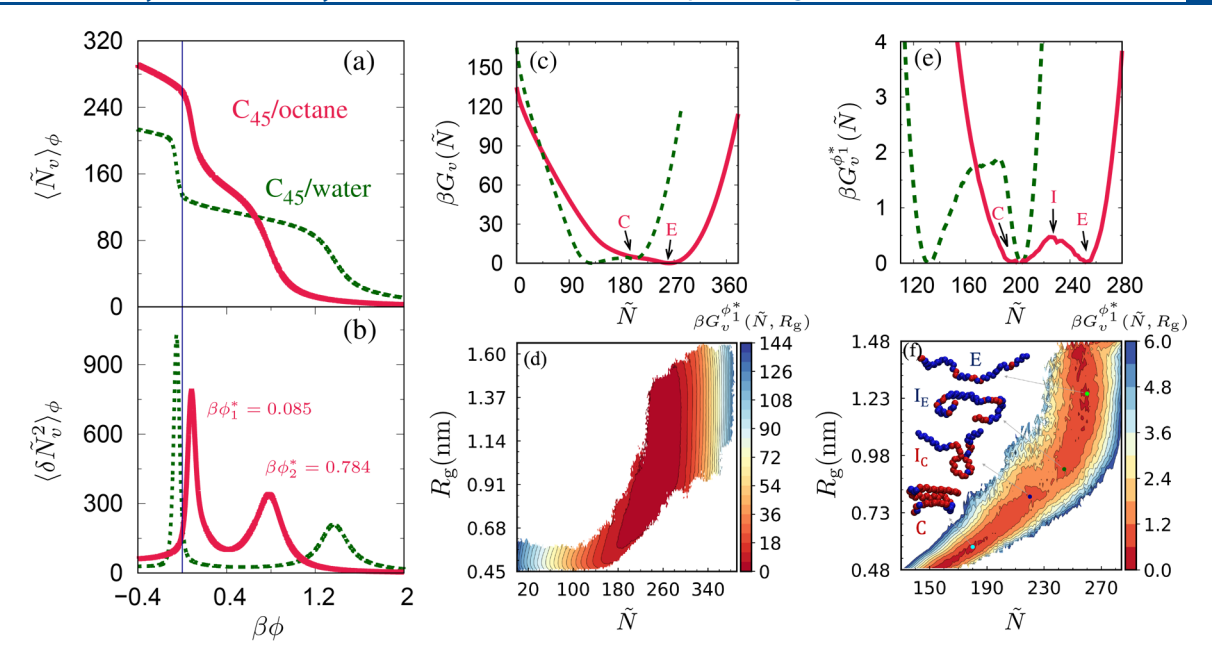


Figure 4. C_{45} polymer solvated in octane. (a) The average number of solvent heavy atoms, $\langle \tilde{N}_{\nu} \rangle_{\phi}$, in the solvation shell, ν , of the C_{45} polymer is shown as a function of the strength, ϕ , of the linear biasing potential, $U_{\phi} = \phi \tilde{N}_{\nu}$. For the C_{45} polymer solvated in both octane (red, solid line) and in water (green, dashed line), two sharp drops in $\langle \tilde{N}_{\nu} \rangle_{\phi}$ are observed as ϕ is increased; the vertical line (blue) depicts $\phi = 0$. (b) Correspondingly, the susceptibility, $-\partial \langle \tilde{N}_{\nu} \rangle_{\phi} / \partial (\beta \phi) = \langle \delta \tilde{N}_{\nu}^2 \rangle_{\phi}$, displays two peaks in both cases; the locations of the peaks, ϕ_1^* and ϕ_2^* , are included for octane. In contrast with C_{45} in water, $\phi_1^* > 0$ for C_{45} solvated in octane, suggesting that polymer is in its extended state at equilibrium ($\phi = 0$). (c) The free energetics of solvent number fluctuations, $G_{\nu}(\tilde{N})$, in the solvation shell of the C_{45} polymer are shown, and the locations of the collapsed (C) and extended (E) states of the polymer are denoted with arrows. In octane, the extended state (high \tilde{N}) is stable, whereas the collapsed state (low \tilde{N}) is unstable. (d) The two-dimensional free energy landscape, $G_{\nu}(\tilde{N})$, $G_{\nu}(\tilde{N})$, of solvent fluctuations in the ϕ_1^* -ensemble, display two distinct basins that are separated by a barrier. (f) The two-dimensional free energy landscape, $G_{\nu}^{\phi^*}(\tilde{N})$, shown here for the C_{45} polymer solvated in octane, as well as the representative configurations of the polymer, are qualitatively similar to those for C_{45} in water (Figure 3b).

(I_E and I_C), and the collapsed basin (C). In addition to depicting the conformation of the polymer, the snapshots also highlight the localized hydration of the individual polymer beads; hydrated beads are shown in blue, whereas dehydrated beads are colored red. Such simulation snapshots, which are also included in Movies S1-S4 of the Supporting Information, further elucidate the pathways involved in polymer collapse. In particular, as it approaches the saddle point, the polymer adopts a partially collapsed conformation with some of its monomers clustering together but remaining well-hydrated (Figure 3b, snapshot I_E); crossing the saddle point region requires the dehydration of such a cluster (Figure 3b, snapshot I_C). Thus, the formation of a sufficiently large hydrophobic cluster and its dehydration represent the barrier to polymer collapse. These findings highlight the importance of collective water density fluctuations in facilitating polymer collapse.

Our results also lend support to the observations of ten Wolde and Chandler, ¹⁵ who studied the collapse of a purely repulsive, idealized hydrophobic polymer using a coarsegrained model of water, and those of Miller et al., ¹⁶ who studied the same polymer using atomistic simulations; both studies found that the formation of a critical nonpolar cluster and its dewetting represent the barrier to polymer collapse. Moreover, the agreement between these studies, performed on ideal hydrophobic polymers, and our results, obtained using realistic polymers, which have favorable dispersion interactions

with water, highlight that weak polymer—water attractions do not qualitatively alter the polymer hydration landscape. 52

3.4. Polymer Collapse in Octane. We now study the solvation of the hydrophobic C₄₅ polymer in octane, a nonpolar solvent, and draw comparisons to the solvation of the polymer in water. In Figure 4a, we plot the response of the average number of solvent heavy atoms, $\langle \tilde{N}_{\nu} \rangle_{\phi}$, in the polymer solvation shell, ν , to the strength, ϕ , of the linear biasing potential, $U_{\phi} = \phi \tilde{N}_{\nu}$, and in Figure 4b, we plot the corresponding susceptibility, $-\partial \langle \tilde{N}_{\nu} \rangle_{\phi} / \partial (\beta \phi) = \langle \delta \tilde{N}_{\nu}^2 \rangle_{\phi}$. Once again, two sharp drops are observed in $\langle \tilde{N}_{\nu} \rangle_{\!\phi}$ with increasing ϕ , and correspondingly, two peaks are seen in $\langle \delta \tilde{N}_{\nu}^{2} \rangle_{\phi}$ at ϕ -values denoted by ϕ_{1}^{*} and ϕ_{2}^{*} . The configurations of C_{45} in octane, shown for three select \tilde{N}_{ν} -values in Figure S2 of the Supporting Information, suggest that the transitions at ϕ_1^* and ϕ_2^* , once again, correspond to polymer collapse and the dewetting of the collapsed polymer. Vertical lines in Figure 4a,b (blue) correspond to ϕ = 0 and highlight that, in contrast with C_{45} in water, ϕ_1^* is positive for C_{45} in octane. Thus, the folding (or collapse) free energy, $\Delta G_{\text{fold}} \approx \phi_1^* (\tilde{N}_{\text{E}} - \tilde{N}_{\text{C}})$, must also be positive, suggesting that, in octane, the extended state of C₄₅ is stable relative to its collapsed state. Figure 4b also shows that the dewetting of the collapsed polymer occurs

at a lower ϕ_2^* -value in octane than in water; this observation can be readily rationalized in terms of the smaller liquid—vapor surface tension of octane, which makes it easier to form cavities.⁵³

The unbiased free energy landscapes, $G_{\nu}(\tilde{N})$ and $G_{\nu}(\tilde{N}, R_{\sigma})$, for C₄₅ in octane, are shown in Figure 4c,d, and the conformational free energy landscape, $G_v(R_g)$, is included as Figure S3 of the Supporting Information. Apart from the fact that the collapsed state is metastable with respect to the extended state, with $\beta G_{\rm fold} = 4.5$, the landscapes are qualitatively similar to those for C_{45} in water (Figure 2). The corresponding free energy landscapes in the ϕ_1^* -ensemble are shown in Figure 4e,f. As with C_{45} in water, the collapsed (C) and extended (E) states are degenerate in the ϕ_1^* -ensemble for C_{45} in octane, and a barrier is observed at intermediate \tilde{N} and $R_{\rm g}$. Although the barrier height is somewhat lower for C_{45} in octane (relative to water), both the $G_{\nu}^{\phi_1^*}(\tilde{N}, R_{\sigma})$ landscape and representative configurations of the polymer (Figure 4f) suggest that polymer collapse in octane proceeds through mechanistic pathways, which are remarkably similar to those in water (Figure 3b). In particular, as in water, the collapse of the C₄₅ polymer in octane also proceeds through the formation of a sufficiently large cluster and its desolvation.

To understand these similarities, we first recognize that polymer collapse involves the solvent-mediated assembly of well-solvated subunits, which are smaller than 1 nm, into a cluster that is larger than 1 nm in size. According to the Lum-Chandler-Weeks theory of hydrophobicity, the solvation free energy of the former scales as their excluded volume, whereas the solvation free energy of the latter scales as its surface area; this interplay between solvation at small and large length scales is responsible for the emergence of a critical cluster, which must be nucleated for the collapse transition to proceed. Interestingly, a solute size-dependent crossover in solvation free energies has also been observed in nonpolar solvents, such as octane. Although the corresponding solvophobic effect, experienced by solutes in nonpolar solvents, is expected to be weaker than the hydrophobic effect, our results suggest that it may nevertheless be responsible for the qualitative similarities between the polymer collapse pathways in water and in octane.

4. CONCLUSIONS AND OUTLOOK

Using the recently developed dynamic indirect umbrella sampling (INDUS) method for sampling the number of solvent molecules, \tilde{N}_{ν} , in the dynamical solvation shell of a flexible solute, here we study the coil-to-globule or collapse transition of a hydrophobic polymer solvated in water and in the nonpolar solvent, octane. We find that an unfavorable potential, which perturbs \tilde{N}_{ν} , can trigger the collapse transition, and that the requisite potential strength quantifies the relative stabilities of the collapsed and extended states. To understand the interplay between polymer solvation and conformation, we characterize the free energy landscape of the system as a function of both the number of solvent molecules, \tilde{N}_{ν} , in the polymer solvation shell, and its radius of gyration, $R_{\rm g}$. We find that the bottleneck to polymer collapse is the formation of a critical nonpolar cluster and its desolvation. In particular, assisted by thermal fluctuations, an extended polymer must first adopt a relatively compact configuration, which features a

sufficiently large nonpolar cluster; the cluster must then undergo collective dewetting before the rest of the polymer can collapse.

In agreement with previous studies on ideal hydrophobic polymers, ^{15,16} our findings thus confirm the presence of slow solvent coordinates in the coil-to-globule transition and highlight the importance of collective solvent density fluctuations in overcoming the corresponding barriers. In contrast with water, which is a poor solvent for the hydrophobic polymer, the nonpolar solvent, octane, is expected to be a good solvent for the polymer. Interestingly, we find that the mechanistic details of the collapse transition in octane are nevertheless remarkably similar to that in water. Our results suggest that the size-dependent crossover in solvation free energies, which has been observed not just in water⁵⁷ but also in nonpolar solvents, such as octane, ^{53,61} may underpin the similarities in the polymer collapse pathways observed in these two solvents.

A characterization of the free energetics of water density fluctuations in static volumes, both in bulk water^{56,63} and in the vicinity of surfaces, 64-67 has provided numerous insights into the collective, solvent-mediated hydrophobic effects, ranging from micelle formation and interfacial assembly, to superhydrophobicity and protein interactions. ^{68–72} By characterizing the free energetics of solvent density fluctuations in the dynamic solvation shells of conformationally flexible molecules, we hope that our work will similarly pave the way for a richer understanding of the conformational transitions 73,74 and the phase behavior^{75,76} of large classes of interesting solutes, ranging from hydrocarbons and polymers, to peptides and nucleic acids. 33,34,77 Our approach is also likely to shed light into how cosolutes (e.g., osmolytes, salts, etc.), which have a propensity to be included or excluded from the vicinity of a polymer, might modulate the solvation of a polymer as well as its conformational landscape. $^{78-84}$

ASSOCIATED CONTENT

Supporting Information

The Supporting Information is available free of charge at https://pubs.acs.org/doi/10.1021/acs.jpcb.1c02191.

Plots supporting Figures 2 and 4 (PDF)

Movie supporting Figure 3 showing a collection of 60 simulation snapshots shown for the C_{45} polymer in its extended basin, E, i.e., with its hydration waters in the range $\tilde{N}_{\nu} \in [202, 207]$ and its radius of gyration in the range $R_{\rm g} \in [1.23 \text{ nm}, 1.27 \text{ nm}]$ (hydrated beads are colored blue, whereas dehydrated beads are colored red) (MP4)

Movie supporting Figure 3 showing a collection of 60 simulation snapshots shown for the C_{45} polymer in its transition region, I_E , i.e., with its hydration waters in the range $\tilde{N}_{\nu} \in [196, 202]$ and its radius of gyration in the range $R_g \in [0.89 \text{ nm}, 0.93 \text{ nm}]$ (hydrated beads are colored blue, whereas dehydrated beads are colored red) (MP4)

Movie supporting Figure 3 showing a collection of 60 simulation snapshots shown for the C_{45} polymer in its transition region, I_C , i.e., with its hydration waters in the range $\tilde{N}_{\nu} \in [172, 178]$ and its radius of gyration in the range $R_g \in [0.78 \text{ nm}, 0.82 \text{ nm}]$ (hydrated beads are colored blue, whereas dehydrated beads are colored red) (MP4)

Movie supporting Figure 3 showing a collection of 60 simulation snapshots shown for the C_{45} polymer in its collapsed basin, C, i.e., with its hydration waters in the range $\tilde{N}_{\nu} \in [127, 133]$ and its radius of gyration in the range $R_{\rm g} \in [0.50$ nm, 0.54 nm] (hydrated beads are colored blue, whereas dehydrated beads are colored red) (MP4)

AUTHOR INFORMATION

Corresponding Author

Amish J. Patel — Department of Chemical and Biomolecular Engineering, University of Pennsylvania, Philadelphia, Pennsylvania 19104, United States; occid.org/0000-0001-6482-543X; Email: amish.patel@seas.upenn.edu

Authors

- Debdas Dhabal Department of Chemical and Biomolecular Engineering, University of Pennsylvania, Philadelphia, Pennsylvania 19104, United States
- Zhitong Jiang Department of Chemical and Biomolecular Engineering, University of Pennsylvania, Philadelphia, Pennsylvania 19104, United States
- Akash Pallath Department of Chemical and Biomolecular Engineering, University of Pennsylvania, Philadelphia, Pennsylvania 19104, United States

Complete contact information is available at: https://pubs.acs.org/10.1021/acs.jpcb.1c02191

Notes

The authors declare no competing financial interest.

ACKNOWLEDGMENTS

A.J.P. gratefully acknowledges financial support from the National Science Foundation (NSF Grants CBET-1652646, CHE-1665339, and DMR-1720530), and awards from the Alfred P. Sloan Research Foundation (FG-2017-9406) and the Camille and Henry Dreyfus Foundation (TC-19-033). D.D. was supported by NSF Grant CHE-1665339.

■ REFERENCES

- (1) Hu, D.; Yu, J.; Wong, K.; Bagchi, B.; Rossky, P. J.; Barbara, P. F. Collapse of stiff conjugated polymers with chemical defects into ordered, cylindrical conformations. *Nature* **2000**, *405*, 1030–1033.
- (2) Ashbaugh, H. S.; Paulaitis, M. E. Monomer hydrophobicity as a mechanism for the LCST behavior of poly (ethylene oxide) in water. *Ind. Eng. Chem. Res.* **2006**, *45*, 5531–5537.
- (3) Lin, B.; Martin, T. B.; Jayaraman, A. Decreasing Polymer Flexibility Improves Wetting and Dispersion of Polymer-Grafted Particles in a Chemically Identical Polymer Matrix. ACS Macro Lett. **2014**, *3*, 628–632.
- (4) Pandav, G.; Pryamitsyn, V.; Errington, J.; Ganesan, V. Multibody Interactions, Phase Behavior, and Clustering in Nanoparticle—Polyelectrolyte Mixtures. *J. Phys. Chem. B* **2015**, *119*, 14536—14550.
- (5) Sharma, A.; Liu, L.; Parameswaran, S.; Grayson, S. M.; Ashbaugh, H. S.; Rick, S. W. Design of Amphiphilic Polymers via Molecular Dynamics Simulations. *J. Phys. Chem. B* **2016**, *120*, 10603–10610.
- (6) Thirumalai, D.; Lorimer, G. H. Chaperonin-Mediated Protein Folding. *Annu. Rev. Biophys. Biomol. Struct.* **2001**, *30*, 245–269.
- (7) Matysiak, S.; Debenedetti, P. G.; Rossky, P. J. Dissecting the Energetics of Hydrophobic Hydration of Polypeptides. *J. Phys. Chem. B* **2011**, *115*, 14859–14865.

- (8) Carmichael, S. P.; Shell, M. S. A New Multiscale Algorithm and Its Application to Coarse-Grained Peptide Models for Self-Assembly. *J. Phys. Chem. B* **2012**, *116*, 8383–8393.
- (9) Bellissent-Funel, M.-C.; Hassanali, A.; Havenith, M.; Henchman, R.; Pohl, P.; Sterpone, F.; van der Spoel, D.; Xu, Y.; Garcia, A. E. Water Determines the Structure and Dynamics of Proteins. *Chem. Rev.* **2016**, *116*, 7673–7697.
- (10) Liu, L.; Parameswaran, S.; Sharma, A.; Grayson, S. M.; Ashbaugh, H. S.; Rick, S. W. Molecular dynamics simulations of linear and cyclic amphiphilic polymers in aqueous and organic environments. *J. Phys. Chem. B* **2014**, *118*, 6491–6497.
- (11) DuBay, K. H.; Bowman, G. R.; Geissler, P. L. Fluctuations within Folded Proteins: Implications for Thermodynamic and Allosteric Regulation. *Acc. Chem. Res.* **2015**, *48*, 1098–1105.
- (12) Peter, E. K.; Shea, J.-E.; Pivkin, I. V. Coarse kMC-based replica exchange algorithms for the accelerated simulation of protein folding in explicit solvent. *Phys. Chem. Chem. Phys.* **2016**, *18*, 13052–13065.
- (13) Lawrence, C. W.; Kumar, S.; Noid, W. G.; Showalter, S. A. Role of Ordered Proteins in the Folding-Upon-Binding of Intrinsically Disordered Proteins. *J. Phys. Chem. Lett.* **2014**, *5*, 833–838.
- (14) Ferguson, A. L.; Panagiotopoulos, A. Z.; Debenedetti, P. G.; Kevrekidis, I. G. Systematic determination of order parameters for chain dynamics using diffusion maps. *Proc. Natl. Acad. Sci. U. S. A.* **2010**, *107*, 13597–13602.
- (15) ten Wolde, P. R.; Chandler, D. Drying-induced hydrophobic polymer collapse. *Proc. Natl. Acad. Sci. U. S. A.* **2002**, *99*, 6539–6543.
- (16) Miller, T. F.; Vanden-Eijnden, E.; Chandler, D. Solvent coarse-graining and the string method applied to the hydrophobic collapse of a hydrated chain. *Proc. Natl. Acad. Sci. U. S. A.* **2007**, *104*, 14559—14564.
- (17) Berne, B. J.; Weeks, J. D.; Zhou, R. Dewetting and Hydrophobic Interaction in Physical and Biological Systems. *Annu. Rev. Phys. Chem.* **2009**, *60*, 85–103.
- (18) Setny, P.; Baron, R.; Michael Kekenes-Huskey, P.; McCammon, J. A.; Dzubiella, J. Solvent fluctuations in hydrophobic cavity-ligand binding kinetics. *Proc. Natl. Acad. Sci. U. S. A.* **2013**, 110, 1197–1202.
- (19) Remsing, R. C.; Xi, E.; Vembanur, S.; Sharma, S.; Debenedetti, P. G.; Garde, S.; Patel, A. J. Pathways to dewetting in hydrophobic confinement. *Proc. Natl. Acad. Sci. U. S. A.* **2015**, *112*, 8181–8186.
- (20) Tiwary, P.; Mondal, J.; Morrone, J. A.; Berne, B. Role of Water and Steric Constraints in the Kinetics of Cavity—Ligand Unbinding. *Proc. Natl. Acad. Sci. U. S. A.* **2015**, *112*, 12015—12019.
- (21) Lum, K.; Chandler, D.; Weeks, J. D. Hydrophobicity at small and large length scales. *J. Phys. Chem. B* **1999**, *103*, 4570–4577.
- (22) Athawale, M. V.; Goel, G.; Ghosh, T.; Truskett, T. M.; Garde, S. Effects of lengthscales and attractions on the collapse of hydrophobic polymers in water. *Proc. Natl. Acad. Sci. U. S. A.* **2007**, 104, 733–738.
- (23) Goel, G.; Athawale, M. V.; Garde, S.; Truskett, T. M. Attractions, Water Structure, and Thermodynamics of Hydrophobic Polymer Collapse. *J. Phys. Chem. B* **2008**, *112*, 13193–13196.
- (24) Xi, E.; Marks, S. M.; Fialoke, S.; Patel, A. J. Sparse sampling of water density fluctuations near liquid-vapor coexistence. *Mol. Simul.* **2018**, *44*, 1124–1135.
- (25) Athawale, M. V.; Sarupria, S.; Garde, S. Enthalpy-Entropy Contributions to Salt and Osmolyte Effects on Molecular-Scale Hydrophobic Hydration and Interactions. *J. Phys. Chem. B* **2008**, *112*, 5661–5670.
- (26) Stirnemann, G.; Kang, S.-g.; Zhou, R.; Berne, B. J. How force unfolding differs from chemical denaturation. *Proc. Natl. Acad. Sci. U. S. A.* **2014**, *111*, 3413–3418.
- (27) Mondal, J.; Halverson, D.; Li, I. T. S.; Stirnemann, G.; Walker, G. C.; Berne, B. How osmolytes influence hydrophobic polymer conformations: A unified view from experiment and theory. *Proc. Natl. Acad. Sci. U. S. A.* **2015**, *112*, 9270–9275.
- (28) Nayar, D.; van der Vegt, N. F. A. Cosolvent Effects on Polymer Hydration Drive Hydrophobic Collapse. *J. Phys. Chem. B* **2018**, *122*, 3587–3595.

- (29) Jamadagni, S. N.; Godawat, R.; Dordick, J. S.; Garde, S. How Interfaces Affect Hydrophobically Driven Polymer Folding. *J. Phys. Chem. B* **2009**, *113*, 4093–4101.
- (30) Jamadagni, S. N.; Godawat, R.; Garde, S. How Surface Wettability Affects the Binding, Folding, and Dynamics of Hydrophobic Polymers at Interfaces. *Langmuir* **2009**, *25*, 13092–13099.
- (31) Vaitheeswaran, S.; Chen, J.; Thirumalai, D. Hydrophobic and ionic-interactions in bulk and confined water with implications for collapse and folding of proteins. *J. Stat. Phys.* **2011**, *145*, 276–292.
- (32) Vembanur, S.; Patel, A. J.; Sarupria, S.; Garde, S. On the Thermodynamics and Kinetics of Hydrophobic Interactions at Interfaces. J. Phys. Chem. B 2013, 117, 10261–10270.
- (33) Zerze, G. H.; Mullen, R. G.; Levine, Z. A.; Shea, J.-E.; Mittal, J. To What Extent Does Surface Hydrophobicity Dictate Peptide Folding and Stability near Surfaces? *Langmuir* **2015**, *31*, 12223–12230.
- (34) Jiang, Z.; Remsing, R. C.; Rego, N. B.; Patel, A. J. Characterizing Solvent Density Fluctuations in Dynamical Observation Volumes. *J. Phys. Chem. B* **2019**, *123*, 1650–1661.
- (35) Patel, A. J.; Varilly, P.; Jamadagni, S. N.; Hagan, M. F.; Chandler, D.; Garde, S. Sitting at the Edge: How Biomolecules use Hydrophobicity to Tune Their Interactions and Function. *J. Phys. Chem. B* **2012**, *116*, 2498–2503.
- (36) Patel, A. J.; Garde, S. Efficient Method To Characterize the Context-Dependent Hydrophobicity of Proteins. *J. Phys. Chem. B* **2014**, *118*, 1564–1573.
- (37) Patel, A. J.; Varilly, P.; Chandler, D. Fluctuations of Water near Extended Hydrophobic and Hydrophilic Surfaces. *J. Phys. Chem. B* **2010**, *114*, 1632–1637.
- (38) Patel, A. J.; Varilly, P.; Chandler, D.; Garde, S. Quantifying Density Fluctuations in Volumes of All Shapes and Sizes Using Indirect Umbrella Sampling. *J. Stat. Phys.* **2011**, *145*, 265–275.
- (39) Souaille, M.; Roux, B. Extension to the weighted histogram analysis method: combining umbrella sampling with free energy calculations. *Comput. Phys. Commun.* **2001**, *135*, 40–57.
- (40) Shirts, M. R.; Chodera, J. D. Statistically optimal analysis of samples from multiple equilibrium states. *J. Chem. Phys.* **2008**, *129*, 124105.
- (41) Zhu, F.; Hummer, G. Convergence and error estimation in free energy calculations using the weighted histogram analysis method. *J. Comput. Chem.* **2012**, *33*, 453–465.
- (42) Tan, Z.; Gallicchio, E.; Lapelosa, M.; Levy, R. M. Theory of binless multi-state free energy estimation with applications to protein-ligand binding. *J. Chem. Phys.* **2012**, *136*, 144102.
- (43) Xi, E.; Remsing, R. C.; Patel, A. J. Sparse Sampling of Water Density Fluctuations in Interfacial Environments. *J. Chem. Theory Comput.* **2016**, *12*, 706–713.
- (44) Hess, B.; Kutzner, C.; van der Spoel, D.; Lindahl, E. GROMACS 4: Algorithms for Highly Efficient, Load-Balanced, and Scalable Molecular Simulation. *J. Chem. Theory Comput.* **2008**, *4*, 435–447.
- (45) Bussi, G.; Donadio, D.; Parrinello, M. Canonical Sampling through Velocity Rescaling. *J. Chem. Phys.* **2007**, *126*, 014101.
- (46) Parrinello, M.; Rahman, A. Polymorphic Transitions in Single Crystals: A New Molecular Dynamics Method. *J. Appl. Phys.* **1981**, *52*, 7182–7190.
- (47) Martin, M. G.; Siepmann, J. I. Transferable Potentials for Phase Equilibria. 1. United-Atom Description of n-Alkanes. *J. Phys. Chem. B* **1998**, *102*, 2569–2577.
- (48) Berendsen, H. J. C.; Grigera, J. R.; Straatsma, T. P. The Missing Term in Effective Pair Potentials. *J. Phys. Chem.* **1987**, *91*, 6269–6271
- (49) Miyamoto, S.; Kollman, P. A. Settle: An analytical version of the SHAKE and RATTLE algorithm for rigid water models. *J. Comput. Chem.* **1992**, *13*, 952–962.
- (50) Essmann, U.; Perera, L.; Berkowitz, M. L.; Darden, T.; Lee, H.; Pedersen, L. G. A Smooth Particle Mesh Ewald Method. *J. Chem. Phys.* **1995**, *103*, 8577–8593.

- (51) Rego, N. B.; Xi, E.; Patel, A. J. Protein Hydration Waters are Susceptible to Unfavourable Perturbations. *J. Am. Chem. Soc.* **2019**, 141, 2080–2086.
- (52) Remsing, R. C.; Patel, A. J. Water density fluctuations relevant to hydrophobic hydration are unaltered by attractions. *J. Chem. Phys.* **2015**, *142*, 024502.
- (53) Wu, E.; Garde, S. Lengthscale-Dependent Solvation and Density Fluctuations in n-Octane. *J. Phys. Chem. B* **2015**, *119*, 9287–9294
- (54) Li, I. T. S.; Walker, G. C. Signature of hydrophobic hydration in a single polymer. *Proc. Natl. Acad. Sci. U. S. A.* **2011**, *108*, 16527–16532.
- (55) Garde, S.; Patel, A. J. Unraveling the hydrophobic effect, one molecule at a time. *Proc. Natl. Acad. Sci. U. S. A.* **2011**, *108*, 16491–16492.
- (56) Hummer, G.; Garde, S.; Garcia, A. E.; Pohorille, A.; Pratt, L. R. An Information Theory Model of Hydrophobic Interactions. *Proc. Natl. Acad. Sci. U. S. A.* **1996**, *93*, 8951–8955.
- (57) Rajamani, S.; Truskett, T. M.; Garde, S. Hydrophobic hydration from small to large lengthscales: Understanding and manipulating the crossover. *Proc. Natl. Acad. Sci. U. S. A.* **2005**, 102, 9475–9480.
- (58) Varilly, P.; Patel, A. J.; Chandler, D. An improved coarse-grained model of solvation and the hydrophobic effect. *J. Chem. Phys.* **2011**, *134*, 074109.
- (59) Vaikuntanathan, S.; Rotskoff, G.; Hudson, A.; Geissler, P. L. Necessity of Capillary Modes in a Minimal Model of Nanoscale Hydrophobic Solvation. *Proc. Natl. Acad. Sci. U. S. A.* **2016**, *113*, E2224–E2230.
- (60) Xi, E.; Patel, A. J. The hydrophobic effect, and fluctuations: the long and the short of it. *Proc. Natl. Acad. Sci. U. S. A.* **2016**, 113, 4549–4551.
- (61) Huang, D. M.; Chandler, D. Cavity formation and the drying transition in the Lennard-Jones fluid. *Phys. Rev. E: Stat. Phys., Plasmas, Fluids, Relat. Interdiscip. Top.* **2000**, *61*, 1501–1506.
- (62) Cerdeirina, C. A.; Debenedetti, P. G.; Rossky, P. J.; Giovambattista, N. Evaporation Length Scales of Confined Water and Some Common Organic Liquids. *J. Phys. Chem. Lett.* **2011**, 2, 1000–1003.
- (63) Garde, S.; Hummer, G.; Garcia, A. E.; Paulaitis, M. E.; Pratt, L. R. Origin of Entropy Convergence in Hydrophobic Hydration and Protein Folding. *Phys. Rev. Lett.* **1996**, *77*, 4966–4968.
- (64) Godawat, R.; Jamadagni, S. N.; Garde, S. Characterizing hydrophobicity of interfaces by using cavity formation, solute binding, and water correlations. *Proc. Natl. Acad. Sci. U. S. A.* **2009**, *106*, 15119–15124.
- (65) Acharya, H.; Vembanur, S.; Jamadagni, S. N.; Garde, S. Mapping Hydrophobicity at the Nanoscale: Applications to Heterogeneous Surfaces and Proteins. *Faraday Discuss.* **2010**, *146*, 353–365.
- (66) Rotenberg, B.; Patel, A. J.; Chandler, D. Molecular Explanation for Why Talc Surfaces can be Both Hydrophilic and Hydrophobic. *J. Am. Chem. Soc.* **2011**, 133, 20521–20527.
- (67) Jamadagni, S. N.; Godawat, R.; Garde, S. Hydrophobicity of Proteins and Interfaces: Insights from Density Fluctuations. *Annu. Rev. Chem. Biomol. Eng.* **2011**, *2*, 147–171.
- (68) Maibaum, L.; Dinner, A. R.; Chandler, D. Micelle Formation and the Hydrophobic Effect. *J. Phys. Chem. B* **2004**, *108*, 6778–6781.
- (69) Patel, A. J.; Varilly, P.; Jamadagni, S. N.; Acharya, H.; Garde, S.; Chandler, D. Extended surfaces modulate hydrophobic interactions of neighboring solutes. *Proc. Natl. Acad. Sci. U. S. A.* **2011**, *108*, 17678–17683
- (70) Prakash, S.; Xi, E.; Patel, A. J. Spontaneous recovery of superhydrophobicity on nanotextured surfaces. *Proc. Natl. Acad. Sci. U. S. A.* **2016**, *113*, 5508–5513.
- (71) Xi, E.; Venkateshwaran, V.; Li, L.; Rego, N.; Patel, A. J.; Garde, S. Hydrophobicity of proteins and nanostructured solutes is governed by topographical and chemical context. *Proc. Natl. Acad. Sci. U. S. A.* **2017**, *114*, 13345–13350.

- (72) Rego, N. B.; Xi, E.; Patel, A. J. Identifying hydrophobic protein patches to inform protein interaction interfaces. *Proc. Natl. Acad. Sci. U. S. A.* **2021**, *118*, No. e2018234118.
- (73) Rodriguez-Ropero, F.; Hajari, T.; van der Vegt, N. F. A. Mechanism of Polymer Collapse in Miscible Good Solvents. *J. Phys. Chem. B* **2015**, *119*, 15780–15788.
- (74) Budkov, Y. A.; Kolesnikov, A. L.; Georgi, N.; Kiselev, M. G. A flexible polymer chain in a critical solvent: Coil or globule? *Europhys. Lett.* **2015**, *109*, 36005.
- (75) Dignon, G. L.; Zheng, W.; Best, R. B.; Kim, Y. C.; Mittal, J. Relation between single-molecule properties and phase behavior of intrinsically disordered proteins. *Proc. Natl. Acad. Sci. U. S. A.* **2018**, *115*, 9929–9934.
- (76) Bharadwaj, S.; van der Vegt, N. F. A. Does Preferential Adsorption Drive Cononsolvency? *Macromolecules* **2019**, *52*, 4131–4138
- (77) Duboué-Dijon, E.; Fogarty, A. C.; Hynes, J. T.; Laage, D. Dynamical Disorder in the DNA Hydration Shell. *J. Am. Chem. Soc.* **2016**, *138*, 7610–7620.
- (78) Mountain, R. D.; Thirumalai, D. Molecular dynamics simulations of end-to-end contact formation in hydrocarbon chains in water and aqueous urea solution. *J. Am. Chem. Soc.* **2003**, *125*, 1950–1957.
- (79) Ganguly, P.; van der Vegt, N. F. A.; Shea, J.-E. Hydrophobic Association in Mixed Urea—TMAO Solutions. *J. Phys. Chem. Lett.* **2016**, 7, 3052—3059.
- (80) Nayar, D.; van der Vegt, N. F. A. The Hydrophobic Effect and the Role of Cosolvents. *J. Phys. Chem. B* **2017**, *121*, 9986–9998.
- (81) Remsing, R. C.; Xi, E.; Patel, A. J. Protein Hydration Thermodynamics: The Influence of Flexibility and Salt on Hydrophobin II Hydration. *J. Phys. Chem. B* **2018**, *122*, 3635–3646.
- (82) Zhang, Y.; Cremer, P. S. Chemistry of Hofmeister Anions and Osmolytes. *Annu. Rev. Phys. Chem.* **2010**, *61*, 63–83.
- (83) Okur, H. I.; Hladílková, J.; Rembert, K. B.; Cho, Y.; Heyda, J.; Dzubiella, J.; Cremer, P. S.; Jungwirth, P. Beyond the Hofmeister series: ion-specific effects on proteins and their biological functions. *J. Phys. Chem. B* **2017**, *121*, 1997–2014.
- (84) Mukherji, D.; Watson, M. D.; Morsbach, S.; Schmutz, M.; Wagner, M.; Marques, C. M.; Kremer, K. Soft and Smart: Cononsolvency-Based Design of Multiresponsive Copolymers. *Macromolecules* **2019**, *52*, 3471–3478.